Cascaded Sagnac loops embedded with two polarization maintaining photonic crystal fibers for highly-sensitive strain measurement

Qiang Liu, Liang Xing, Zhaoxia Wu, Yongqing Fu, Shuguang Li, Pingsheng Xue, Waipang Ng, Qiang Wu, and Richard Binns

***Abstract*—A strain sensor based on cascaded Sagnac loops with two PMPCFs has been experimentally demonstrated. Air holes distributed on the cross section of PMPCF go through the whole fiber which make the special fiber more sensitive to ambient force compared with conventional optical fiber. The lengths of the two PMPCFs are close, but not the same, to form envelopes on the total output spectrum and then obtain high resolution to the detected parameter by Vernier effect. The influences of the difference in length of the two PMPCFS on spectral envelopes are discussed. As the length of the PMPCF in reference loop increases, free spectrum range of the cascaded Sagnac loops (or envelope period) and magnification decrease. The sensitivities of this strain sensor are calculated by tracking upper- and lower-envelope. Results reveal that its average sensitivity is up to 45.15 pm/$\mu\varepsilon$ and the corresponding resolution is 0.44 $\mu\varepsilon$ as strain varies from 0 to 2000 $\mu\varepsilon$. Compared with a single Sagnac loop, the sensitivity magnification is about 28.94. The sensing characteristics of a conventional PMF are studied to compare with the PMPCF. Moreover, reversibility has also been proved to possess low error rate. In short, the fiber strain sensor possesses high sensitivity and great reversibility.**

***Index Terms*—Strain sensor; Cascaded Sagnac loops; Photonic crystal fiber; Vernier effect.**

I. Introduction

FIBER optic sensors [1]–[6] have attracted much attention in recent years with the development of optoelectronic technology. They have numerous outstanding merits, such as anti-electromagnetic interference, immunity to corrosion, high sensitivity, quick response, light weight, remote operation and real-time monitoring. The application fields of fiber-optic sensors are very wide including chemical industry, electric power, civil engineering, biomedicine and so on. Meanwhile diversified physical parameters can be measured by fiber-optic sensors, such as vibration [7], rotation [8], flow rate [9], acceleration [10], and strain [11], [12], etc.

Fiber-optic strain sensors have been widely investigated for applications in many fields such as physiological parameters (heart rate, respiratory frequency) and structural health monitoring (aircraft, ground deformation, landslide, ground fissure) [13]–[20]. Many air holes are distributed on the cross section of PCFs and go through the whole fiber which make the fiber easy to deform and more sensitive to ambient force compared with conventional optical fibers made of all solid materials. Moreover, polarization maintaining PCFs (PMPCFs) are less sensitive to temperature and the cross-talk between strain and temperature is avoidable, because the background materials of the PMPCFs are only pure silica and air holes whose thermal dependence is very low, while conventional polarization maintaining fibers (PMFs), such as panda and bow-tie PMFs, are more sensitive to temperature due to that they usually have boron-doped parts whose thermal sensitive coefficient is much higher than pure silica [21].

Dong et al. realized a strain sensor by splicing a piece of PCF with two sections of thin core fibers (TCFs), a Mach-Zehnder interferometer was formed by the TCF-PCF-TCF structure and the strain sensitivity was only -1.89 pm/$\mu\varepsilon$ [22]. Tang et al. demonstrated the sensing characteristics of a triple-core PCF with a strain sensitivity of -29.8 pm/$\mu\varepsilon$, meanwhile the coupling coefficient among the three cores was studied as the fiber was stretched [23]. Dong et al. realized a strain sensor by utilizing a Sagnac interferometer inserted with a PCF, the low strain sensitivity of 0.23 pm/$\mu\varepsilon$ was obtained and the detecting range was up to 32 mε [21]. Choi et al. proposed a PCF based Mach-Zehnder interferometer and achieved the strain sensitivity of -2.16 pm/$\mu\varepsilon$ [24]. A hollow-core PCF strain sensor based on Sagnac interferometer was proposed by Kim et al., temperature and strain were measured simultaneously and the strain sensitivity was only -0.81 pm/$\mu\varepsilon$ [25]. Han et al. proposed a strain sensor with the sensitivity of 25 pm/$\mu\varepsilon$ based on PCF Sagnac interferometer and the zero-group-birefringence effect was utilized to enhance sensitivity [26]. The sensitivities of the fiber strain sensors mentioned above are not sufficiently high. Hence, it is needful to take advantage of special methods to enhance detection resolution.

Vernier effect is usually applied by vernier caliper which utilizes small scale difference between main ruler and vernier

This work was supported by the National Natural Science Foundation of China (Grant No. 51907017), Key Science and Technology Research Projects of Higher Education Institutions in Hebei Province of China (Grant No. ZD2019304), Fundamental Research Funds for the Central Universities of China (Grant No. N182304011) and China National Fund for Studying Abroad.

Q. Liu, L. Xing, Z. Wu, and P. Xue are with State Key Laboratory of Synthetical Automation for Process Industries, School of Control Engineering, Northeastern University at Qinhuangdao, 066004, Peoples Republic of China (e-mail: liuqiang@neuq.edu.cn; xingliang@stumail.neu.edu.cn; y-suwzx@126.com; 1901906@stu.neu.edu.cn).

Y. Fu, W. Ng, Q. Wu, and R. Binns, are with Faculty of Engineering and Environment, Northumbria University, Newcastle Upon Tyne, NE1 8ST, United Kingdom (e-mail: richard.fu@northumbria.ac.uk; wai-pang.ng@northumbria.ac.uk; qiang.wu@northumbria.ac.uk; richard.binns@northumbria.ac.uk).

S. Li is with Key Laboratory of Metastable Materials Science and Technology, College of Science, Yanshan University, Qinhuangdao 066004, Peoples Republic of China (e-mail: shuguangli@ysu.edu.cn).

to improve measurement accuracy. In recent years, Vernier effect has been used for optical detection [27]–[35]. Liao et al. proposed the cascaded Mach-Zehnder interferometers based on offset splicing between single-mode fibers and the maximum amplification of sensitivity was nearly 9 [27]. Xu et al. realized a temperature sensor based on cascaded fiber rings with the sensitivity amplification of 30 [28]. Deng et al. utilized the Fabry-Perot interferometers formed by femtosecond laser to generate Vernier effect and the strain sensitivity of 28.11 pm/$\mu\varepsilon$ was achieved [29]. Li et al. reported a fiber modal interferometer with Vernier effect induced by birefringence effect, and the human cardiac troponin was detected with a detecting limit of 1 ng/mL [30]. Shao et al. realized a temperature sensor based on Vernier effect and conventional PMF, while the conventional PMF is less sensitive to ambient force compared with PMPCF [31]. We realized a highly sensitive temperature sensor based on Vernier effect and PMPCF, the special fiber was assumed to be filled with temperature sensitive liquid whose temperature sensitive coefficient is much higher than that of the fiber background material of silica and the sensitivity was improved by the combination of Vernier effect and sensitive liquid by simulation [34]. It can be seen Vernier effect in optics has been demonstrated as an effective method to enhance sensitivity.

In this paper, we propose a highly sensitive strain sensor based on the combination of Vernier effect and PMPCF. PMPCF is more sensitive to ambient force due to the porous structure compared with conventional PMF. Two PMPCFs with length difference are embedded into cascaded Sagnac loops to generate envelopes on the total output spectrum and achieve high detection resolution to the detected parameter by Vernier effect. One Sagnac loop is employed as a sensing part and the other Sagnac loop as a reference part. A PMPCF in sensing loop is clamped on two three-dimensional-displacement platforms which are utilized to modulate strain. The influences of the length of the PMPCF in reference loop on envelopes are discussed and the sensitivity of the cascaded Sagnac loops are calculated by tracking upper- and lower-envelope. Results exhibit that an average sensitivity of 45.15 pm/$\mu\varepsilon$ is achieved as strain varies from 0 to 2000 $\mu\varepsilon$. While the sensitivities of the single Sagnac loop based on PMPCF or conventional PMF are just 1.56 and 0.95 pm/$\mu\varepsilon$. The reversibility is also demonstrated to have a good effect. This fiber strain sensor with high sensitivity and great reversibility is competitive in strain sensing field.

II. Principle and Experimental Setup

A. PMPCF structure

Cross section of the PMPCF (PMPCF-125-03, Shanghai Fsphotonics Technology Ltd, China) is shown in Fig. 1. It can be seen that there are many air holes distributed on its cross section in a triangular lattice, meanwhile the air holes go through the whole fiber. The diameter of the two large air holes is larger than the other air holes which means the difference in refractive index between horizontal- and vertical-direction exists and the PMPCF possesses high birefringence. If birefringence is low, there may be no dips appearing in the considerable wavelength range for a single Sagnac loop or envelopes are not obvious for the cascaded Sagnac loops. The total diameter of the special fiber is about 125 μm and the background material is pure fused silica.

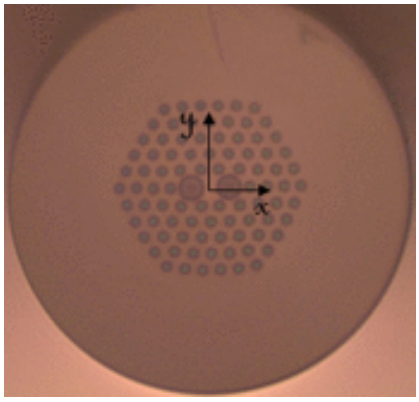

Fig. 1. Cross section of the PMPCF. Air holes are distributed on the cross section in a triangular lattice. The diameter of the two large air holes is larger than the other air holes to obtain high birefringence.

B. Single Sagnac loop

Sagnac effect was first discovered and experimentally demonstrated by Sagnac in 1913. It reveals the relationship between optical path difference between the two beams propagating in opposite directions and rotation speed. As a fiber ring rotates at an angular velocity by the axis perpendicular to the ring plane, an optical path difference of the two beams traveling in opposite directions is generated, meanwhile the optical path difference is proportional to rotational angular velocity [36], [37]. Fiber-optic sensors based on Sagnac interferometer have many advantages, such as compact structure, high stability, self-balance and so on. Schematic diagram of the PMPCF strain sensor based on a single Sagnac loop is shown in Fig. 2. One beam of light emitted by a supercontinuous light source (SCLS) passes through a 3 dB optical coupler (OC) and is divided into two beams which possess the same intensity and transmit in opposite directions. The

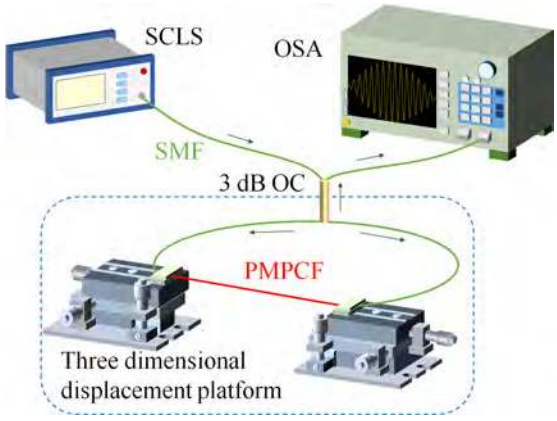

Fig. 2. Schematic diagram of the experimental set-up for strain measurement based on a PMPCF Sagnac loop. A PMPCF is clamped on two three-dimensional-displacement platforms to modulate strain.

phase difference between the two beams exists due to the birefringence effect of the PMPCF as they transmit back to the optical coupler, therefore interference will occur.

Transmission spectrum can be calculated by [38]

$$T = \frac{1 - cos(2\pi BL/\lambda)}{2}, \tag{1}$$

where L is the length of the PMPCF, λ is the wavelength of light. Birefringence B can be calculated by

$$B = n_{\mathrm{y}} - n_{\mathrm{x}}. \tag{2}$$

Birefringence B describes the refractive index difference between the two fiber modes in fast- and slow-axis of the special fiber. In our experiment, PMPCF and conventional PMF are all utilized respectively. Transmission spectrum is recorded by an optical spectrum analyzer (OSA).

Free spectrum range (FSR) of a single Sagnac loop can be calculated by

$$FSR = \frac{\lambda^2}{BL}. \tag{3}$$

It is easy to find that FSR of the single Sagnac loop is inversely proportional to birefringence B and the length L of PMPCF, thereby free spectrum range can be modulated by changing birefringence B and fiber length L. When the fiber is subjected to lateral strain (ε=$\Delta L/L$), there will be deformation for the fiber due to elasto-optical effect. The birefringence B and fiber length L are all changed, therefore phase difference $\Delta\varphi$ will undergo changes which can be described by

$$\Delta\varphi = \frac{2\pi(B\Delta L + \Delta BL)}{\lambda}, \tag{4}$$

It is easy to obtain ΔL and the change in birefringence ΔB can be calculated by

$$\Delta B = \Delta n_{\mathrm{y}} - \Delta n_{\mathrm{x}}. \tag{5}$$

As well as the changes in refractive index caused by photoelastic effect can be obtained by [21]

$$\Delta n_{\mathrm{x,y}} = p^{\mathrm{x,y}} n_{\mathrm{x,y}} \varepsilon, \tag{6}$$

where $p^{\mathrm{x,y}}$ are the effective photoelastic constants in x- and y-axis. The change of phase difference gives rise to the shift of resonance wavelength which can be calculated by

$$\Delta\lambda = \frac{FSR\Delta\varphi}{2\pi}. \tag{7}$$

By substituting Eqs. (2)-(6) into Eq. (7), the relation between the change of wavelength and strain can be described by

$$\Delta\lambda = \lambda(1 + p')\varepsilon, \tag{8}$$

where $p' = (p^{\mathrm{y}} n^{\mathrm{y}} - p^{\mathrm{x}} n^{\mathrm{x}})/B$ is a constant for a certain fiber. Therefore we can come to a conclusion that the change of wavelength $\Delta\lambda$ is proportional to strain ε which means that strain magnitude can be obtained accurately by tracking the variation of resonance wavelength.

C. Cascaded Sagnac loops

Figure 3 shows the schematic diagram of the experimental set-up of the cascaded Sagnac loops embedded with two PMPCFs for strain measurement. Sagnac loop on the left serves as a reference section and the other loop on the right serves as a sensing section. Two PMPCFs with small difference in length are inserted into Sagnac loops respectively. One beam of light emitted by SCLS first passes through a 3dB OC with a splitting ratio of 1:1 and is divided into two beams of light which possess the same intensity and transmit in opposite directions. The two beams can also interfere as they return to the optical coupler. A single mode fiber is utilized to connect the reference- and sensing-section. The output light from the reference loop is utilized as the input light of the sensing loop where the interference will occur again. The total output spectrum is the superposition of the spectra of the two single Sagnac loops and the output light last transmits to OSA used to record datum.

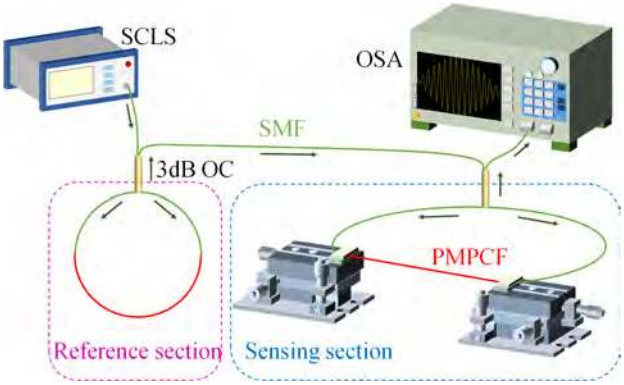

Fig. 3. Schematic diagram of the experimental set-up for strain measurement based on the cascaded PMPCF Sagnac loops. Two PMPCFs with small difference in length are inserted into the two Sagnac loops respectively. The left Sagnac loop serves as a reference section and the other loop serves as a sensing section. Output light from the reference loop is utilized as the input light of the sensing loop.

The free spectrum ranges of the two Sagnac loops are close, but not the same, because the two PMPCFs possess small difference in length. This gives rise to the appearance of envelopes on the total output spectrum for the cascaded Sagnac loops. The envelope period FSR_{Env} of the cascaded Sagnac loops can be derived by [31]

$$FSR_{\mathrm{Env}} = \frac{FSR_{\mathrm{Ref}} \times FSR_{\mathrm{Sen}}}{|FSR_{\mathrm{Ref}} - FSR_{\mathrm{Sen}}|}, \tag{9}$$

where FSR_{Ref} and FSR_{Sen} are the free spectrum ranges of the reference- and sensing-loop. Sensitivity magnification M compared with single Sagnac loop can be calculated by

$$M = \frac{FSR_{\mathrm{Ref}}}{|FSR_{\mathrm{Ref}} - FSR_{\mathrm{Sen}}|}. \tag{10}$$

It can be seen that M is proportional to FSR_{Ref} and inversely proportional to the absolute value of the difference between the two free spectrum ranges of the reference- and sensing-loop. Thereby the sensitivity of the fiber sensor can be improved by adjusting the free spectrum ranges of the reference- and sensing-loop.

D. Experimental setup

A SCLS (SC-5, Wuhan Yangtze Soton Laser Co., Ltd, China) is utilized as the input light source whose spectral stability is no more than 0.1 dB as wavelength varies from 800 to 1700 nm. Transmission spectrum is recorded by an OSA (AQ6370D, YOKOGAWA, Japan) whose resolution is 20 pm and analyzable wavelength ranges from 600 to 1700 nm. We take advantage of an optical fiber fusion splicer (FITEL, S179C) to splice PMPCFs and single mode fibers. Manual mode is applied to align x- and y-axis of the fibers under a microscope to ensure low splicing loss. Discharge intensity and time are 35 units and 300 ms to avoid air holes collapsing and ensure weld strength. The PMPCF in sensing loop is clamped on two three-dimensional-displacement platforms, one platform remains stationary and the other platform moves horizontally to adjust strain at room temperature.

III. Results and Discussion

A. Single Sagnac loop

1) PMPCF: If the length of the PMPCF in a single Sagnac loop decreases, we see FSR will increase according to Eq. (3) which means that the number of the interference fringes decreases in a considerable wavelength range. Since the total output spectrum of the cascaded Sagnac loops is the superposition of the spectra of the reference- and sensing-loop, the number of the peaks or dips in one envelope period will decrease which will increase measurement error, because we need to fit the curves for the upper- and lower-envelope to obtain the wavelengths corresponding to the peak and valley of the envelope curves which will be discussed in subsection B, section III. If the length of the PMPCF in sensing loop increases, the loss will increase, meanwhile the length of the PMPCF in reference loop has to be increased to obtain good magnification based on Eq. (10), then the loss in reference loop will also increase. To balance Vernier effect and loss, the initial length of the PMPCF in sensing loop is chosen through multiple attempts in the experiments.

The length of 63 cm for the PMPCF is chosen to be embedded into a single Sagnac loop to carry out strain experiments. The PMPCF is clamped on two three-dimensional displacement platforms to modulate strain. Fig. 4(a) shows the transmission spectrum as strain varies from 0 to 2000 $\mu\varepsilon$ with a step of 400 $\mu\varepsilon$. Two dips A and B appear in the considerable wavelength range and free spectrum range is $\sim$3.9 nm. The largest and smallest transmittance are about -36 and -50 dB. Transmittance at the dip wavelengths does not change much with strain changing. Dip A and B red shift as strain increases from 0 to 2000 $\mu\varepsilon$, dip A varies from 1499.1 to 1502.2 nm, dip B moves from 1503.0 to 1506.1 nm, the two dips all shift 3.1 nm and the corresponding sensitivity can reach to 1.55 pm/$\mu\varepsilon$. The strain applied to the fiber results in that birefringence B of the PMPCF changes and the length of the fiber increases which cause interference fringes to shift. The phase difference between the two beams of light will change according to Eq. (4) which leads the two dips to move toward longer wavelength. Fig. 4(b) shows the relation between dip wavelength and strain, the fitted lines are made, and the fitted

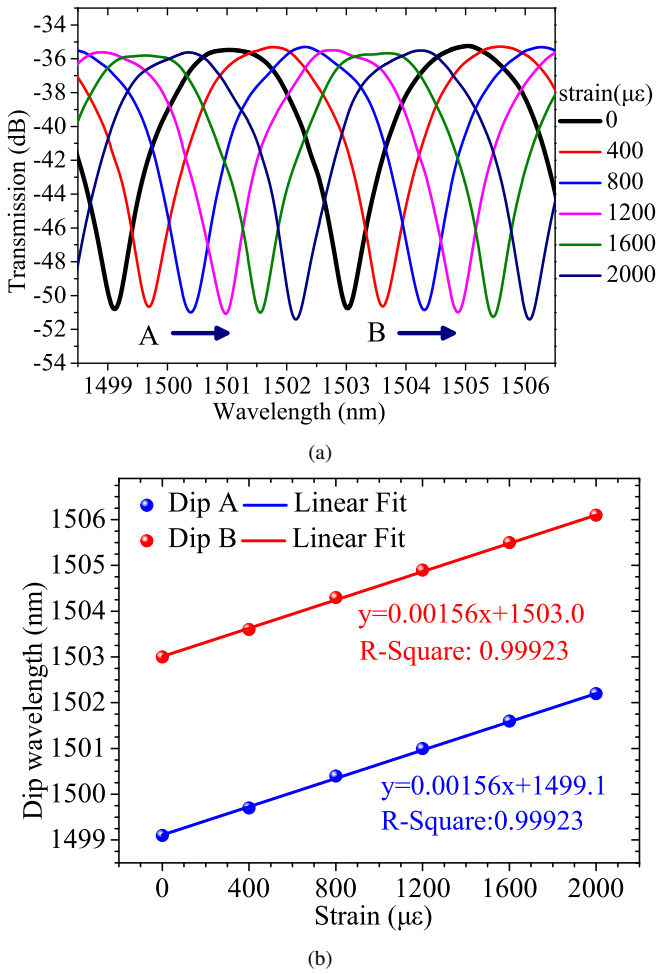

Fig. 4. (a) Experimental transmission spectrum of a single PMPCF Sagnac loop as strain increases from 0 to 2000 $\mu\varepsilon$ with the strain interval of 400 $\mu\varepsilon$. Dip A and B red shift with strain increasing because of the changes in birefringence B and fiber length L. (b) The relation between dip wavelength and strain. The corresponding fitted lines are made. Their average sensitivities are the same and they are only 1.56 pm/$\mu\varepsilon$ for dip A and B.

equations are y=0.00156x+1499.1 and y=0.00156x+1503.0 for dip A and B. It can be seen that they have the same sensitivity of 0.00156 nm/$\mu\varepsilon$ (1.56 pm/$\mu\varepsilon$), meanwhile their R-Squares are also the same and they are 0.99923. The sensitivity of this fiber strain sensor based on a single PMPCF Sagnac loop is low, the detection limit is 12.8 $\mu\varepsilon$ as the resolution of the optical spectrum analyzer is 20 pm.

2) Conventional PMF: The strain experiments based on a conventional PMF (SM15-PS-U25D, Optical Device Sales Engineering Department, 1440, Mutsuzaki, Sakura, Chiba 285-8550, Japan) are conducted to compare with the PMPCF. Fig. 5 shows the transmission spectrum of a single Sagnac loop embedded with a conventional PMF as strain are 0 and 2000 $\mu\varepsilon$. The length of the conventional PMF is set as 140 cm and the free spectrum range of $\sim$3.8 nm is obtained, which is close to that based on the PMPCF, to ensure at the same condition. The dip wavelengths are $\sim$1503.1 and $\sim$1505.0 nm respectively and the sensitivity is calculated to be 0.95 pm/$\mu\varepsilon$ which is lower than that based on the PMPCF. Illustration shows the cross section of the conventional PMF which has a

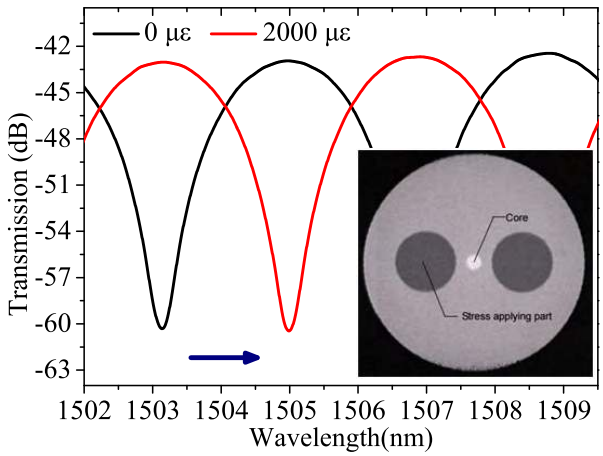

Fig. 5. Experimental transmission spectrum of a single Sagnac loop embedded with a conventional PMF as strain are 0 and 2000 $\mu\varepsilon$. The dip wavelengths are ∼1503.1 and ∼1505.0 nm and the sensitivity is 0.95 pm/$\mu\varepsilon$ which is lower than that based on the PMPCF. Illustration shows the cross section of the conventional PMF.

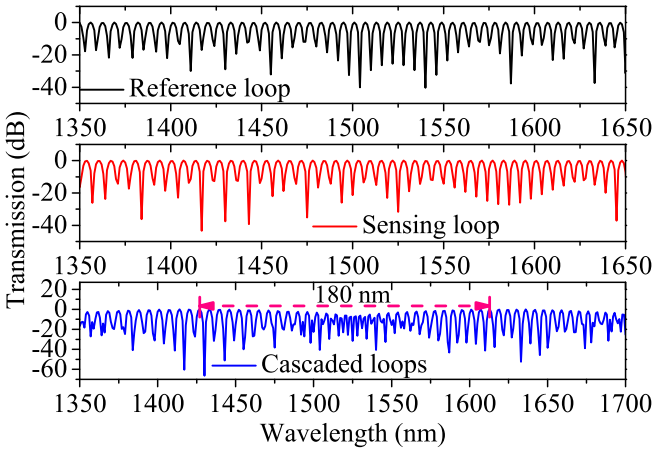

Fig. 6. Simulated transmission spectrum of the reference-, sensing-loop and the cascaded loops from top to bottom. $FSRs$ of the reference- and sensing-loop are nearly the same of ∼6 nm, FSR_{Env} of the cascaded loops is ∼180 nm for the upper envelope. Magnification can reach to 30.

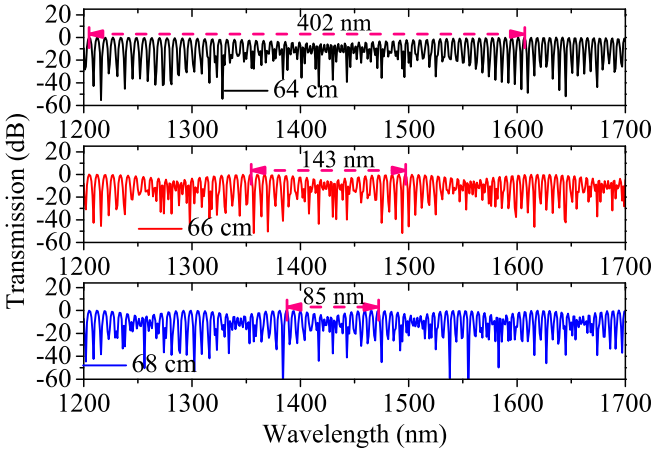

Fig. 7. Simulated transmission spectrum of the cascaded Sagnac loops. The lengths of the PMPCF in reference loop are 64, 66 and 68 cm from top to bottom. The length of the PMPCF in sensing loop is fixt to 63 cm. FSR_{Env} decreases with the fiber length increasing.

superior optical property in polarization-maintaining because of the symmetrical accuracy in cross section and the uniform constitution of stress applying parts. It can be found that the PMPCF is more sensitive to strain than the conventional PMF. Because there are many air holes distributed on the cross section of the PMPCF and they go through the whole fiber, while the conventional PMF is made of all solid materials, the equivalent elasticity modulus of the PMPCF is smaller than the conventional PMF. Since the background materials of the PMPCF only consist of pure silica and air holes, the thermal dependence of the fiber is very low, while the conventional PMFs, such as panda and bow-tie PMFs, usually have boron-doped parts whose thermal sensitive coefficient is much higher than pure silica [21]. In the reference [39], the temperature-insensitivity of a PMPCF Sagnac loop was improved 55 times and the variation of wavelength with temperature was only 0.05 pm/°C, because the temperature coefficient of birefringence in a PCF was 30 times lower than that of a conventional PMF. In the reference [40], a PMPCF obtained 45 times smaller temperature dependence of birefringence than that of a conventional PMF, a birefringence coefficient with temperature was obtained to be dB/dT = -2.0×10^{-9} /°C. Therefore the PMPCF is less sensitive to temperature and the cross-talk between strain and temperature is avoidable.

B. Cascaded Sagnac loops

1) Vernier effect by simulation: We carry out a computational simulation for the cascaded PMPCF Sagnac loops with Vernier effect. The refractive indices of x- and y-polarized modes of the PMPCF are obtained by finite element method. The software Comsol is utilized. Scattering boundary condition is applied and the outer layer of the fiber cladding is set as perfect matching layer (PML) to reduce the reflection of light. The background material of the PMPCF is fused silica whose dispersion relation can be described by Sellmeier equation [41]. The ambient temperature is assumed to be 25 °C. Fig. 6 shows the transmission spectra of the reference-, sensing-loop and the cascaded Sagnac loops. The lengths of the PMPCFs in reference- and sensing-loop are set as 65 and 63 cm respectively. $FSRs$ of the reference- and sensing-loop are nearly the same of ∼6 nm near the wavelength of 1500 nm which is larger than that measured in the experiment, because there are inevitable errors for the structural parameters of the PMPCF measured by a microscope. One envelope period consists of multiple peaks and dips, the two highest peaks in the two neighbouring envelope periods are considered which are at the wavelength of 1433 and 1613 nm respectively and then FSR_{Env} of the total output spectrum is calculated to be ∼180 nm. Magnification can reach to 30 calculated by Eq. (9) and Eq. (10).

Then, the influences of the length of the PMPCF in reference loop on envelopes are analyzed. The transmission spectrum of the cascaded Sagnac loops are shown in Fig. 7 where the lengths of the PMPCF in reference loop are 64, 66

and 68 cm, and the length of the PMPCF in sensing loop is fixt to 63 cm. It can be seen that FSR_{Env} decreases as the length of the PMPCF in reference loop increases which can be explained by Eq. (9). FSR_{Env} are 402, 143 and 85 nm as the lengths of the PMPCF in reference loop are 64, 66 and 68 cm. Magnification M will decrease as the length of the PMPCF in reference loop increases based on Eq. (10) which can be rewritten into M=1/|1-$FSR_{\mathrm{Sen}}/FSR_{\mathrm{Ref}}$|, it can be found that the sensitivity magnification is related to the factor of $FSR_{\mathrm{Sen}}/FSR_{\mathrm{Ref}}$. Since the length of the PMPCF in sensing loop is shorter than the PMPCF in reference loop, FSR_{Sen} is larger than FSR_{Ref} which means $FSR_{\mathrm{Sen}}/FSR_{\mathrm{Ref}}$ is larger than 1. As the length of the PMPCF in reference loop increases, FSR_{Ref} decreases, the denominator of the equation increases, then the magnification will decrease. We also find that full width at half maximum (FWHM) is decreased with the length increasing. Synthesizing the above analysis, we set the length of the PMPCF in reference loop to conduct the following experiments.

2) Sensing characteristics in experiments: Firstly, the strain experiments of the cascaded Sagnac loops embedded with two PMPCFs are conducted. The lengths of the PMPCFs in reference- and sensing-loop are set as 65 and 63 cm respectively. The difference in FSR of the two Sagnac loops is about 0.1 nm. Fig. 8(a) shows the total output spectrum as strain varies from 0 to 2000 $\mu\varepsilon$ with the strain interval of 400 $\mu\varepsilon$. The considerable wavelength varies from 1400 to 1675 nm. It is easy to see that the output spectrum red shifts with strain increasing, because the transmission spectrum of the reference loop is fixed, while that of the sensing loop red shifts with strain increasing which leads the superposition spectrum to red shift. The peaks or dips can be connected to form upper- or lower-envelope which are tracked to analyze strain sensing characteristics. The fitted curves between transmittance and wavelengths corresponding to (b) the peaks and (c) dips in one envelope period are made and the fitting polynomial orders are 2 and 7 respectively. We find FWHM of the lower envelope is much narrower than the upper envelope. The relations between wavelengths corresponding to the peak of the upper envelope (peak of the fitted function of the upper envelope), and the valley of the lower envelope (valley of the fitted function of the lower envelope) and strain are shown in illustration. The wavelength of the peak varies from 1505.98 to 1580.55 nm and that of the valley changes from 1512.63 to 1600.42 nm. The fitted lines are made and the fitted equations are y=0.03783x+1504.2251 and y=0.04515x+1513.417 for the upper- and lower-envelope which means the average sensitivities are 37.83 and 45.15 pm/$\mu\varepsilon$ respectively. The relations between sensitivity and strain are also shown in illustration. It can be seen that the change of sensitivity with strain is not regular for the upper envelope, and the sensitivity increases firstly and then decreases with strain increasing for the lower envelope. The sensitivity of the lower envelope is higher than the upper envelope, because the profile of the envelope is not completely symmetric along y-axis direction in one envelope period as shown in the references [29], [30], [32], [33], the tilt angle of the envelope increases as strain increases, and the upper envelope tilts to shorter wavelength, while the lower envelope tilts to longer wavelength which results in that the

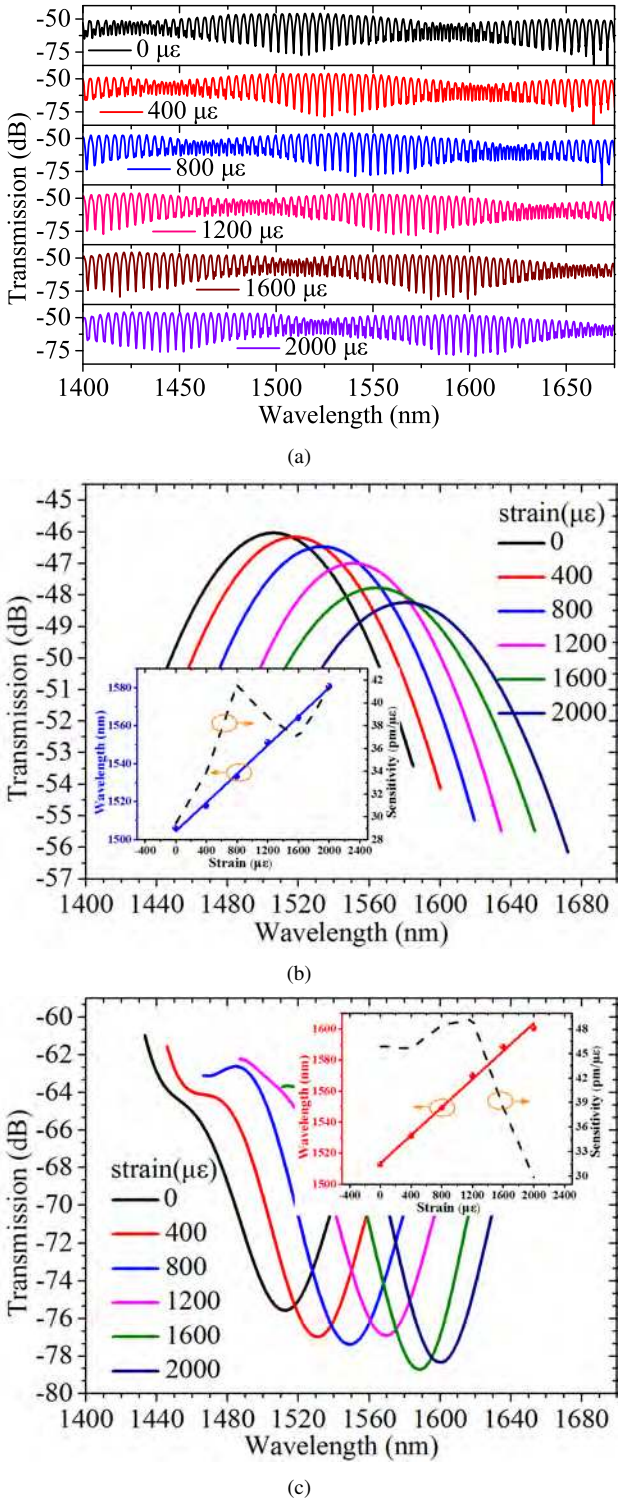

Fig. 8. (a) Experimental transmission spectrum of the cascaded Sagnac loops embedded with two PMPCFs as strain varies from 0 to 2000 $\mu\varepsilon$. Fitted curves between transmittance and wavelengths corresponding to (b) the peaks and (c) dips in one envelope period. The relations between wavelengths corresponding to the peak of the upper envelope (peak of the fitted function of the upper envelope), valley of the lower envelope (valley of the fitted function of the lower envelope) and strain, and the relations between sensitivity and strain are shown in illustration. The corresponding fitted lines are made and the average sensitivities are up to 37.83 and 45.15 pm/$\mu\varepsilon$.

TABLE I
PERFORMANCE COMPARISON BETWEEN OURS AND PREVIOUS WORKS

Ref	Fiber stype	Linearity	Detection range($\mu\varepsilon$)	S(pm/$\mu\varepsilon$)
[11]	MMF	0.994	0-1000	-2.6
[21]	PCF	0.9996	0-32,000	0.23
[22]	PCF	0.9989	0-4000	-1.89
[23]	PCF	0.996	0-1000	-29.8
[24]	PCF	– –	0-3250	-2.28
[25]	PCF	– –	0-1000	-0.81
[26]	PCF	– –	61	25
[29]	SMF	0.99965	0-1400	28.11
[42]	LPFG	– –	0-3100	20
[43]	LPFG	– –	0-500	-5.62
[44]	PCF	0.9889	0-4000	2.92
Ours	PCF	0.99673	0-2000	37.83
		0.99464	0-2000	45.15

(MMF and S represent multimode fiber and sensitivity respectively.)

sensitivity of the lower envelope is higher than the upper envelope. If the same strain is applied to the two PMPCFs in reference- and sensing-loop, the tilt angle can be reduced. The transmission spectra of the reference- and sensing-loop all shift as strain is applied, while one spectrum moves much quicker, similarly the total output spectrum will shift. We call this phenomenon like-Vernier effect, but the sensitivity will be reduced. Sensitivity has been improved by 28.94 times compared with the single Sagnac loop. R-Squares are up to 0.99673 and 0.99464. The detection limit of this strain sensor can be as low as 0.44 $\mu\varepsilon$ provided the resolution of optical spectrum analyzer is 20 pm. Table 1 shows the performance comparison between our work and some previous works and it can be seen the sensitivities of our proposed strain sensor are much higher than the others.

Then, the reversibility of the optical fiber strain sensor based on the cascaded Sagnac loops embedded with two PMPCFs is investigated. A strain goes down step by step from 2000 to 0 $\mu\varepsilon$ with the strain internal of 400 $\mu\varepsilon$ by reversing a platform knob. The total output spectra are also recorded by an optical spectrum analyzer, while they are not presented here, we directly present the fitted curves for the upper- and lower-envelope. Fig. 9(a) shows the fitted curves between transmittance and wavelengths corresponding to the peaks in one envelope period with the fitting polynomial order of 2. As the strain decreases, the curve shifts to short wavelength and the transmittance increases. Fig. 9(b) reveals the fitted curves between transmittance and wavelengths corresponding to the dips in one envelope period with the fitting polynomial order of 7. Similarly the curve shifts to short wavelength with strain decreasing, while the transmittance is not changed regularly. Fig. 9(c) displays the relations between wavelengths corresponding to the peak of the upper envelope, the valley of the lower envelope and strain. Fitted lines are also made and the fitted equations are y=0.0405x+1496.8655 and y=0.04752x+1505.308 for the upper- and lower-envelope which means the average sensitivities of the reverse measurement can reach to 40.50 and 47.52 pm/$\mu\varepsilon$. R-Squares are 0.99238 and 0.99902 separately. There is a little difference of the sensitivities between the forward- and reverse-measurement which indicates the strain sensor possesses great reversibility. The PMPCF in sensing loop is clamped on two three-dimensional-displacement platforms and the fiber is straightened. As the strain applied to the fiber increases, the PMPCF is stretched and its length increases, meanwhile the PMPCF on clamping positions slide slightly due to the elastic force during the process of the experiment, which means the fiber length between the two displacement platforms increases slightly. The slide length for the forward measurement is longer than that for the reverse measurement, because the strain is continuously increased for the forward measurement, while that is continuously decreased for the reverse measurement, therefore the actual strain applied to the fiber for the forward measurement is a little smaller than that for the reverse measurement and then the strain sensitivities in the reverse direction are a little higher than that in the forward direction.

Finally, results of the cascaded Sagnac loops embedded with two conventional PMFs are given to compare with PMPCFs. Fig. 10 shows the transmission spectra as the strain applied to the fiber are 0 and 2000 $\mu\varepsilon$. The experimental conditions are the same as the single Sagnac loop embedded with a conventional PMF. The difference in FSR of the two Sagnac loops is about 0.1 nm to ensure at the same condition with the PMPCF. It can be seen the optical spectrum red shifts as the strain increases. The fitted curves are made for the upper envelopes with the fitting polynomial order of 2. The wavelengths corresponding to the peaks of the upper envelopes are 1483.5 and 1510.1 nm as the strain are 0 and 2000 $\mu\varepsilon$

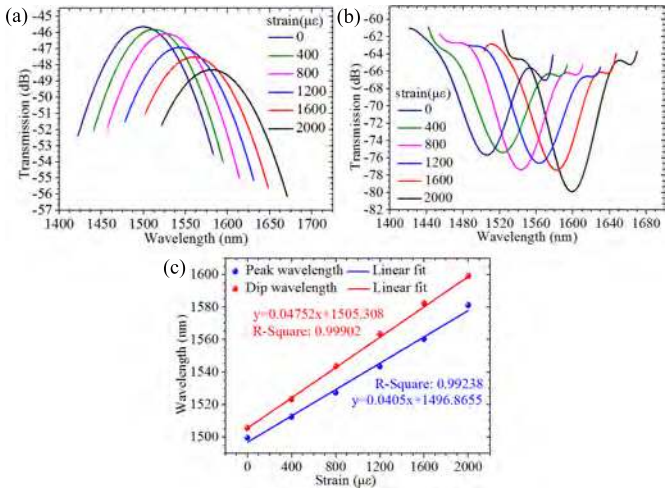

Fig. 9. Experimental results of the optical fiber strain sensor based on the cascaded Sagnac loops embedded with two PMPCFs as the strain decreases from 2000 to 0 $\mu\varepsilon$. Fitted curves between transmittance and wavelengths corresponding to (a) the peaks and (b) dips in one envelope period. (c) The relations between wavelengths corresponding to the peak of the upper envelope, dip of the lower envelope and strain. The sensitivities are 40.50 and 47.52 pm/$\mu\varepsilon$.

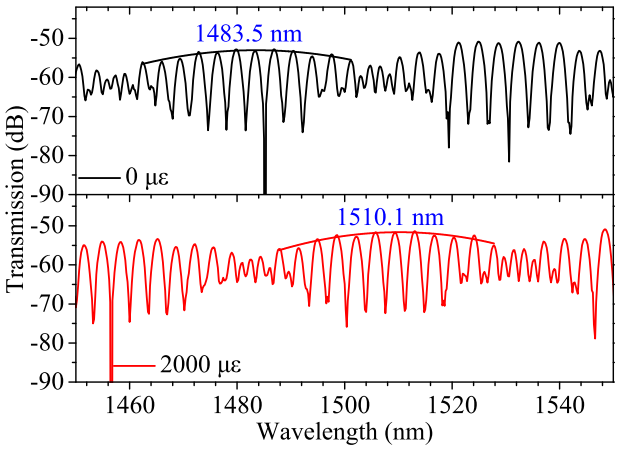

Fig. 10. Experimental transmission spectrum of the cascaded Sagnac loops embedded with two conventional PMFs as the strain are 0 and 2000 $\mu\varepsilon$. The fitted curves for the upper envelopes are made. The sensitivity is only 13.3 pm/$\mu\varepsilon$.

which means the sensitivity is only 13.3 pm/$\mu\varepsilon$ which is much lower than that based on the PMPCFs.

IV. Conclusion

A highly sensitive fiber strain sensor based on the combination of Vernier effect and PMPCF has been proposed and experimentally demonstrated. Two PMPCFs with small difference in length are respectively embedded into cascaded Sagnac loops to enhance sensitivity by employing Vernier effect. The total output spectrum of the cascaded Sagnac loops appears envelopes with a period of ∼162 nm. The strain sensitivities are up to 37.83 and 45.15 pm/$\mu\varepsilon$ by tracking upper- and lower-envelope as strain varies from 0 to 2000 $\mu\varepsilon$. As the resolution of optical spectrum analyzer is 20 pm, the detection limit of this strain sensor is 0.44 $\mu\varepsilon$. While the sensitivity is only 1.56 pm/$\mu\varepsilon$ by the single Sagnac loop embedded with a PMPCF. The sensitivity of the PMPCF is much higher than that of the conventional PMF. In addition, we demonstrate that the sensitivities of the forward- and reverse-measurement possess little difference. Due to the advantages of high sensitivity and great reversibility, the fiber strain sensor is competitive in strain sensing field.

V. Acknowledgement

The authors thank Christopher Markwell from Northumbria University in United Kingdom for his revision in language.

References

[1] T. G. Giallorenzi, J. A. Bucaro, A. Dandridge, G. H. Sigel, J. H. Cole, S. C. Rashleigh, and R. G. Priest, "Optical fiber sensor technology," *IEEE T. Microw. Theory*, vol. 30, pp. 472-511, 1982.

[2] C. Preininger, I. Klimant, and O. S. Wolfbeis, "Optical fiber sensor for biological oxygen demand," *Anal. Chem.*, vol. 66, pp. 1841-1846, 1994.

[3] T. Yoshino, K. Kurosawa, K. Itoh, and T. Ose, "Fiber-optic Fabry-Perot interferometer and its sensor applications," *IEEE T. Microw. Theory*, vol. 30, pp. 1612-1621, 1982.

[4] Y. Zhao, R. J. Tong, F. Xia, and Y. Peng, "Current status of optical fiber biosensor based on surface plasmon resonance," *Biosens. Bioelectron.*, vol. 142, pp. 111505, 2019.

[5] X. Zhou, S. Li, X. Li, X. Yan, X. Zhang, and T. Cheng, "A vectorial analysis of the curvature sensor based on a dual-core photonic crystal fiber," *IEEE T. Instrum. Meas.* 2020. DOI: 10.1109/TIM.2020.2968777

[6] P. Imperatore, G. Persichetti, G. Testa, and R. Bernini, "Continuous liquid level sensor based on coupled light diffusing fibers," *IEEE J. Sel. Top. Quant.*, vol. 26, pp. 1-8, 2020.

[7] J. Villatoro, E. Antonio-Lopez, A. Schlzgen, and R. Amezcua-Correa, "Miniature multicore optical fiber vibration sensor," *Opt. Lett.*, vol. 42, pp. 2022-2025, 2017.

[8] P. Kisala, D. Harasim, and J. Mroczka, "Temperature-insensitive simultaneous rotation and displacement (bending) sensor based on tilted fiber Bragg grating," *Opt. Express*, vol. 24, pp. 29922-29929, 2016.

[9] V. Lien, and F. Vollmer, "Microfluidic flow rate detection based on integrated optical fiber cantilever," *Lab Chip*, vol. 7, pp. 1352-1356, 2007.

[10] T. Yoshino, Y. Sano, D. Ota, K. Fujita, and T. Ikui, "Fiber-Bragg-grating based single axial mode Fabry-Perot interferometer and its strain and acceleration sensing applications," *J. Lightw. Technol.*, vol. 34, pp. 2241-2250, 2016.

[11] K. Tian, G. Farrell, X. F. Wang, W. L. Yang, Y. F. Xin, H. D. Liang, E. Lewis, and P. F. Wang, "Strain sensor based on gourd-shaped single-mode-multimode-single-mode hybrid optical fibre structure," *Opt. Express*, vol. 25, pp. 18885-18896, 2017.

[12] S. Chowdhury, S. Verma, and T. K. Gangopadhyay, "A comparative s-tudy and experimental observations of optical fiber Sagnac interferometric based strain sensor by using different fibers," *Opt. Fiber Technol.*, vol. 48, pp. 283-288, 2019.

[13] L. Dziuda, J. Lewandowski, F. Skibniewski, and G. Nowicki, "Fibre-optic sensor for respiration and heart rate monitoring in the MRI environment," *Procedia Eng.*, vol. 47, pp. 1291-1294, 2012.

[14] A. F. Silva, J. P. Carmo, P. M. Mendes, and J. H. Correia, "Simultaneous cardiac and respiratory frequency measurement based on a single fiber Bragg grating sensor," *Meas. Sci. Technol.*, vol. 22, pp. 075801, 2011.

[15] E. Suaste-Gmez, D. Hernndez-Rivera, A. S. Snchez-Snchez, and E. Villarreal-Calva, "Electrically insulated sensing of respiratory rate and heartbeat using optical fibers," *Sensors*, vol. 14, pp. 21523-21534, 2014.

[16] C. Davis, S. Tejedor, I. Grabovac, J. Kopczyk, and T. Nuyens, "High-strain fiber bragg gratings for structural fatigue testing of military aircraft," *Photonic Sens.*, vol. 2, pp. 215-224, 2012.

[17] I. Garcła, J. Zubia, G. Durana, G. Aldabaldetreku, M. A. Illarramendi, and J. Villatoro, "Optical fiber sensors for aircraft structural health monitoring," *Sensors*, vol. 15, pp. 15494-15519, 2015.

[18] C. C. Zhang, H. H. Zhu, and B. Shi, "Role of the interface between distributed fibre optic strain sensor and soil in ground deformation measurement," *Sci. Rep.*, vol. 6, pp. 36469, 2016.

[19] M. Iten, A. M. Puzrin, and A. Schmid, "Landslide monitoring using a road-embedded optical fiber sensor," *Proc. SPIE*, vol. 6933, pp. 693315, 2008

[20] W. Suo, Y. Lu, B. Shi, H. Zhu, G. Wei, and H. Jiang, "Development and application of a fixed-point fiber-optic sensing cable for ground fissure monitoring," *J. Civ. Struct. Health*, vol. 6, pp. 715-724, 2016.

[21] X. Y. Dong, H. Y. Tam, and P. Shum, "Temperature-insensitive strain sensor with polarization-maintaining photonic crystal fiber based Sagnac interferometer," *Appl. Phys. Lett.*, vol. 90, pp. 151113, 2007.

[22] X. R. Dong, Z. Luo, H. F. Du, X. Y. Sun, K. Yin, and J. A. Duan, "Highly sensitive strain sensor based on a novel Mach-Zehnder mode interferometer with TCF-PCF-TCF structure," *Opt. Laser. Eng.*, vol. 116, pp. 26-31, 2018.

[23] Z. J. Tang, S. Q. Lou, X. Wang, W. Zhang, S. B. Yan, and Z. Xing, "Using mode coupling mechanism in symmetrical triple-core photonic crystal fiber for high performance strain sensing," *IEEE J. Sel. Top. Quant.*, vol. 26, pp. 1-7, 2019.

[24] H. Y. Choi, M. J. Kim, and B. H. Lee, "All-fiber Mach-Zehnder type interferometers formed in photonic crystal fiber," *Opt. Express*, vol. 15, pp. 5711-5720, 2007.

[25] G. Kim, T. Y. Cho, K. Hwang, K. Lee, K. S. Lee, Y. Han, and S. B. Lee, "Strain and temperature sensitivities of an elliptical hollow-core photonic bandgap fiber based on Sagnac interferometer," *Opt. Express*, vol. 17, pp. 2481-2486, 2009.

[26] T. Han, Y. G. Liu, Z. Wang, J. Guo, and J. Yu, "A high sensitivity strain sensor based on the zero-group-birefringence effect in a selective-filling high birefringent photonic crystal fiber," *IEEE Photon. J.*, vol. 10, pp. 1-9, 2017.

[27] H. Liao, P. Lu, X. Fu, X. Jiang, W. J. Ni, D. M. Liu, and J. S. Zhang, "Sensitivity amplification of fiber-optic in-line Mach-Zehnder interferometer sensors with modified Vernier-effect," *Opt. Express*, vol. 25, pp. 26899-26909, 2017.

[28] Z. W. Xu, X. W. Shu, and H. Y. Fu, "Sensitivity enhanced fiber sensor based on a fiber ring microwave photonic filter with the Vernier effect," *Opt. Express*, vol. 25, pp. 21559-21566, 2017.

[29] J. Deng, and D. N. Wang, "Ultra-sensitive strain sensor based on femtosecond laser inscribed in-fiber reflection mirrors and vernier effect," *J. Lightw. Technol.*, vol. 37, pp. 4935-4939, 2019.
[30] K. W. Li, N. Zhang, N. Meng, Y. Zhang, W. C. Zhou, T. Zhang, M. Chen, and L. Wei, "Birefringence induced Vernier effect in optical fiber modal interferometers for enhanced sensing," *Sensor. Actuat. B. Chem.*, vol. 275, pp. 16-24, 2018.
[31] L. Y. Shao, Y. Luo, Z. Zhang, X. Zou, B. Luo, W. Pan, and L. Yan, "Sensitivity-enhanced temperature sensor with cascaded fiber optic Sagnac interferometers based on Vernier-effect," *Opt. Commun.*, vol. 336, pp. 73-76, 2015.
[32] Y. Chang, B. Dong, Y. Ma, J. Wei, Z. Ren, and C. Lee, "Vernier effect-based tunable mid-infrared sensor using silicon-on-insulator cascaded rings," *Opt. Express*, vol. 28, pp. 6251-6260, 2020.
[33] C. Lu, X. Dong, L. Lu, Y. Guan, and S. Ding, "Label free all-fiber static pressure sensor based on vernier effect with temperature compensation," *IEEE Sens. J.*, vol. 20, pp. 4726-4731, 2020.
[34] Q. Liu, L. Xing, S. Yan, L. Lv, and Z. Liu, "Sensing characteristics of photonic crystal fiber Sagnac interferometer based on novel birefringence and Vernier effect," *Metrologia*, vol. 57, pp. 035002, 2020.
[35] Y. Jiang, Y. Yi, G. Brambilla, and P. Wang, "Ultra-high-sensitivity refractive index sensor based on dual-microfiber coupler structure with the Vernier effect," *Opt. Lett.*, vol. 45, pp. 1268-1271, 2020.
[36] H. J. Arditty, and H. C. Leefovre, "Sagnac effect in fiber gyroscopes," *Opt. Lett.*, vol. 6, pp. 401-403, 1981.
[37] D. B. Mortimore, "Fiber loop reflectors," *J. Lightw. Technol.*, vol. 6, pp. 1217-1224, 1988.
[38] Y. Liu, B. Liu, X. Feng, W. Zhang, G. Zhou, S. Yuan, G. Kai, and X. Dong, "High-birefringence fiber loop mirrors and their applications as sensors," *Appl. Opt.*, vol. 44, pp. 2382-2390, 2005.
[39] C. L. Zhao, X. Yang, C. Lu, W. Jin, and M. S. Demokan, "Temperature-insensitive interferometer using a highly birefringent photonic crystal fiber loop mirror," *IEEE Photon. Technol. Lett.*, vol. 16, pp. 2535-2537, 2004.
[40] D. H. Kim, and J. U. Kang, "Sagnac loop interferometer based on polarization maintaining photonic crystal fiber with reduced temperature sensitivity," *Opt. Express*, vol. 12, pp. 4490-4495, 2004.
[41] G. Ghosh, M. Endo, and T. Lwasaki, "Temperature-dependent sellmeier coefficients and chromatic dispersions for some optical fiber glass," *J. Lightw. Technol.*, vol. 12, pp. 1338-1342, 1994.
[42] I. D. Villar, O. Fuentes, F. Chiavaioli, J. M. Corres, and I. R. Matias, "Optimized strain long-period fiber grating (LPFG) sensors operating at the dispersion turning point," *J. Lightw. Technol.*, vol. 36, pp. 2240-2247, 2018.
[43] X. Zhong, Y. Wang, J. Qu, C. Liao, S. Liu, J. Tang, Q. Wang, J. Zhao, K. Yang, and Z. Li, "High-sensitivity strain sensor based on inflated long period fiber grating," *Opt. Lett.*, vol. 39, pp. 5463-5466, 2014.
[44] W. Zhang, S. Lou, X. Wang, S. Yan, Z. Tang, and Z. Xing, "Multi-function sensor based on rectangular-lattice photonic crystal fiber with high pressure sensitivity," *Sensor. Actuat. A: Phys.*, pp. 111987, 2020.

Qiang Liu received the B.S. and Ph.D. degrees from the College of Science, Yanshan University, China, in 2013 and 2018, respectively. Since then, he is a lecturer working in the School of Control Engineering, Northeastern University at Qinhuangdao, China. In 2019, he was awarded 'Excellent Doctoral Thesis of Hebei Province, China'. From January 2020 to now, he is a postdoctor with Faculty of Engineering and Environment, Northumbria University, Newcastle Upon Tyne, United Kingdom. His research interests include fiber optical sensors, polarization filters, fiber splitters, photonic crystal fibers and their applications. He has authored and co-authored more than 50 scientific papers.

Yongqing Fu received the Ph.D. degree from Nanyang Technological University, Singapore, and then worked as a Research Fellow in Singapore-Massachusetts Institute of Technology Alliance, and a Research Associate in University of Cambridge. He is currently a Professor at Northumbria University, UK. He was a Reader in Thin Film Centre in University of West of Scotland, Glasgow, UK, and a lecturer in Heriot-Watt University, Edinburgh, UK. He has extensive experience in smart thin film/materials, biomedical microdevices, energy materials, lab-on-chip, micromechanics, MEMS, nanotechnology, sensors and microfluidics. He has established a worldwide reputation from his pioneer research work on shape memory films, piezoelectric thin films, nanostructured composite/films for applications in MEMS, sensing and renewable energy applications. He has authored and co-authored about 150 refereed international journal papers, one book on thin film shape memory alloys and ten book chapters in these areas. He has been regularly invited as referees for over 30 different international journals, and serves as editorial board member for three international journals.

Shuguang Li received the Ph.D. degree in 2004 from College of Information Science and Engineering, Yanshan University, Qinhuangdao, China. He is currently working in the College of Science at Yanshan University as a Professor. His research interests are new type of photoelectric functional materials and special optical fibers, nonlinear optics and laser frequency conversion. He has authored and co-authored more than 100 scientific papers, patents and conference presentations.

Qiang Wu received the B.S. and Ph.D. degrees from Beijing Normal University and Beijing University of Posts and Telecommunications, Beijing, China, in 1996 and 2004, respectively. From 2004 to 2006, he worked as a Senior Research Associate in City University of Hong Kong. From 2006 to 2008, he took up a research associate post in Heriot-Watt University, Edinburgh, U.K. From 2008 to 2014, he worked as a Stokes Lecturer at Photonics Research Centre, Dublin Institute of Technology, Ireland. He is an Associate Professor / Reader with Faculty of Engineering and Environment, Northumbria University, Newcastle Upon Tyne, United Kingdom. His research interests include optical fiber interferometers for novel optical couplers, nanofibers and sensors, microsphere sensors for bio-chemical sensing, the design and fabrication of fiber Bragg grating devices and their applications for sensing, nonlinear fibre optics, surface plasmon resonant and surface acoustic wave sensors. He has over 200 publications in the area of photonics and holds 3 invention patents. He is an Editorial Board Member of Scientific Reports, Associate Editor of IEEE Sensors Journal and Academic Editor of Journal of Sensors.